



# Novel design of natural double-pass solar air heater for higher thermal performance using vortex generator

S.A. Gandjalikhan Nassab<sup>a,\*</sup> and Y. Sheikhnejad<sup>b</sup>

a. *Department of Mechanical Engineering, School of Engineering, Shahid Bahonar University of Kerman, Kerman, Iran.*

b. *Centre for Mechanical Technology and Automation, Universidade de Aveiro, 3810-193, Aveiro, Portugal.*

Received 15 December 2020; received in revised form 26 January 2021; accepted 1 November 2021

## KEYWORDS

Solar air heaters;  
 Vortex generation;  
 Heat transfer enhancement;  
 Turbulent;  
 Natural convection.

**Abstract.** The present study discusses the effects of flapping flexible vortex generators on two-dimensional turbulent free convection airflow in a double-pass solar air heater. To this end, two thin elastic winglets used as vortex generators were attached to two absorber walls near the inlet section at an attack angle of  $65^\circ$ . This novel concept was elaborated through transient numerical simulation of the flow field based on the finite element method and fluid-solid interaction. In addition, an extensive comparison of four different configurations was made in this study. The absorber and outlet temperatures as well as the flow rate and velocity field were carefully calculated, numerical results of which confirmed the considerable enhancement of thermal performance compared to that of conventional parallel double pass heater. The improvement rate was up to 54% in the case of  $\Delta\bar{T} = \bar{T}_{out} - T_{in}$  from 13 to  $20^\circ\text{C}$  while reducing the flow rate by 33.6%. The present numerical results were validated based on the experimental and numerical data reported in the literature.

© 2022 Sharif University of Technology. All rights reserved.

## 1. Introduction

According to the BP report on the energy outlook for 2030, the world commercial energy consumption will be approximately 17 billion tons of oil and the contribution of all types of Renewable Energies (REs) will possibly reach 7%; hence, there is a considerable gap between energy demand and clean energy production [1]. There is also a significant gap between the total demand and available REs. Extensive studies have been conducted on REs and waste energy harvesting to find a desired solution; however, an urgent need is still felt to promote renewable facilities and commercialize

them to be applied in different related industries. Consequently, further research should be conducted to facilitate the application of RE as an essential pillar of sustainable development and to make it as efficient as possible.

### 1.1. State of the art

Solar Air Heater (SAH) in its general form is an inexpensive heat exchanger that provides high temperature air flow in thermal systems [2,3]. As an important RE facility, it has a wide range of applications in cooking, drying agricultural products, heating process in air conditioning systems, etc. SAHs are found in different types and configurations. Based on their working mechanism, they are divided into two classes of natural and forced SAHs; the former requires no external source for airflow, while the latter uses a blower or induced fan for air motion. The forced SAH, consequently, is more expensive which is used in cases

\*. *Corresponding author.*  
*E-mail address: ganj110@uk.ac.ir (S.A. Gandjalikhan Nassab)*

where a higher flow rate is required. On the contrary, a natural SAH is cheaper and simpler than the forced one which is used in cases where higher outlet-temperature is required. SAHs can have single or double passes depending on configuration. The Double-Pass SAH (DP-SAH) is itself divided into two categories of serial and parallel. The serial version is also known as counter flow since the beginning of the second pass starts at the end of the first one. The serial DP-SAH cannot be natural inherently; therefore, it uses external facilities for its driving force. While its application becomes more expensive, it can provide a higher airflow rate. The Parallel Double-Pass SAH (PDP-SAH), on the other hand, can be found in both natural and forced configurations.

SAH is a popular renewable facility owing to its outstanding features; however, its low thermal performance due to the low thermal conductivity of air and low-speed thick boundary layer has made this renewable facility less attractive [4]. To date, several numerical and experimental scientific papers have been published just to be reminder of such drawbacks and to propose a new solution to enhance the thermal performance of the SAH instead. The ideas suggest the construction of solar heaters in different shapes and configurations. From another point of view, Rayeni and Gandjalikhan Nassab [5] studied the application of radiating gas in SAHs including both single- and double-flow types. Their numerical results revealed that the rate of energy conversion increased in double-flow gas heaters due to gas radiation. Foruzan Nia et al. [6] evaluated the effects of gas radiation on the thermal behavior of solar heaters and found that under the condition of high optical thickness for radiating gas flow, the gas outlet temperature and thermal efficiency would get higher values.

The CFD simulation was employed as an important pillar to examine the SAH performance. Vijayan et al. [7] also carried out a study on this subject and experimentally evaluated the effect of embedding packed bed on the efficiency of solar collectors. Ghritlahre and Verma [8] examined the SAH exergy efficiency through artificial neural network and multi-linear regression for smooth and roughened absorber plates based on the experimental data. Yadav and Sani [9] studied the impact of implementing the jet impingement technique on the SAH performance enhancement. They reported the maximum of 7.58 times enhancement in heat transfer accompanied by a drawback of 9.01 times increase in the friction factor for Reynolds number of 17500. Korpale et al. [10] performed numerical simulations for SAH absorber plate optimization and employed surface modification techniques in a wide range of Reynolds numbers.

As observed in recent publications, the performance of SAH is still among the main concerns of

researchers and scientists all around the world. In [11], the performance enhancement of a single-pass natural solar chimney was evaluated under constant heat flux. They performed a numerical simulation and reported improvement in the thermal performance up to 300% using a passive flapping winglet.

### 1.2. Contribution of this study

To the best of the authors' knowledge, no research study has addressed the performance enhancement of any kind for SAHs through the methodology proposed in this study. Moreover, the present study introduced a new effective concept of heat transfer enhancement in SAH, i.e., embedding the elastic winglet also known as a vortex generator. This approach confers an almost-no-cost method for enhancing the SAH performance. Although this method is considered a passive approach, in contrast to all conventional passive approaches, it is able to actively induce new fluid dynamics using Fluid Solid Interaction (FSI). In addition, the current study exhibits the thermo-hydrodynamic behavior of SAH with VG and made some comparisons between EVG and its main competitor, RVG, to examine its features.

### 1.3. Review literature

In [12,13], numerical simulations of FSI of flexible thin structures with forced and free convection heat transfer were performed and the heat transfer enhancement was confirmed using both passive and active techniques. The mixing effect of VG that oscillates freely without any external force, also called passive method, is considered a more efficient method in terms of energy consumption for heat transfer enhancement since it does not require any external driving force for VG oscillation. Numerous studies have employed passive flapping vortex generators for heat transfer enhancement [14,15]. To the best of the author's knowledge, almost all numerical simulations have been done on flexible elastic winglet based on a 2D geometry [16–18], implying that in this particular area, a 2D model may miss a few dynamic and physical features, yet it considers a transient turbulent model together with an independent refined mesh and stable convergence one, thus yielding reliable results. In order to study this subject further, Li et al. [14] compared three winglets with different moduli of elasticity. Varol and Oztop [19] performed the numerical simulation of the inclined flat-plate solar collector using wavy and flat absorbers in the CFDRC commercial software. They reported considerable heat transfer enhancement to the wavy absorber compared to the flat one. In addition, the effects of porous baffle in SAH and thermal energy storage on SAH performance were discussed in the literature and in [20,21]. Through an extensive review, Oztop et al. [22] classified SAHs into seven groups based on their collector covers, absorber materials, shape of absorbing

**Table 1.** Information on the vortex generator.

Length ( $L_V$ )	Thickness ( $\lambda$ )	Angle ( $\delta$ )	Young modulus	Poison ratio	Density
16.5 mm	1.5 mm	$65^\circ$	0.07 MPa	0.4	1000 kg/m <sup>3</sup>

surfaces, flow pattern, and applications. According to this classification, the considered SAH in this study is a PDP-SAH.

Based on the recent literature review, the vortex generation technique for improving the performance of DP-SAH with natural convective flow has not been examined yet. Lack of information on this subject motivated the authors to put more emphasis on the VGs and increase the thermal efficiency of DP-SAH. In this regard, the current study introduced a flapping thin agitator as a vortex generator inside the duct of PDP-SAH attached to the absorber wall to verify its advantages with regard to enhancing SAH performance and decreasing the temperature of the absorber as the main part under constant Solar Heat Flux (SHF). The main focus of this research is on the PDP version of SAH. From now on, to avoid writing a long-term PDP-SAH, only “SAH” will be used. To show the advantages and disadvantages of the novel configuration, extensive comparisons were made among different configurations, namely (a) SAH+EVG, (b) SAH+RVG, and (c) CSAH.

### 2. Model description

The SAH under study is made of three vertical thin plates, as depicted in Figure 1, and the middle one is considered as an absorber that absorbs the incoming solar radiation. The left one is the glass cover that completely behaves as a transparent element, and the right one is the back wall. The working gas enters from the inlet, and the change of gas density pushes it to the outlet section. Absorber plate is of equal distance to its adjacent walls which makes it exposed to the transmitted radiation from the glass cover, while

the other boundary walls are exposed to the ambience where heat transfer takes place through convection. Two main configurations of SAH are heaters with oscillating EVG. In addition, SAHs with RVG were considered in this paper. The length of SAH is equal to  $L$  and the thickness of the air gap is denoted by  $b$  in Figure 1.

The elastic vortex generators are attached to the absorber and located at the axial section with 0.2 m from the inlet. Table 1 presents the dimensions and mechanical properties of the winglets. Both EVG and RVG have the same dimensions and physical characteristics, except for RVG whose modulus of elasticity is considered high enough, indicating no deflection against the airflow.

### 3. Methodology

The analysis was done considering the oscillating EVG inside the computational domain under transient condition until reaching a semi-steady state while both vibrating EVGs and air outlet bulk temperature exhibited their periodic behaviors. To this end, the continuity, momentum, and energy equations for turbulent natural convection flow were solved numerically and simultaneously by progressing in time from the initial state. The set of governing equations was solved through the COMSOL Multiphysics based on the finite element method. To confirm the validity of the computer solver, the obtained numerical results were validated against the experimental data reported in the relevant literature. According to a study conducted by Singh et al. [23], for free convection flow in SAH, the regime of flow became turbulent with the approximate value of Rayleigh number of  $10^{10}$ .

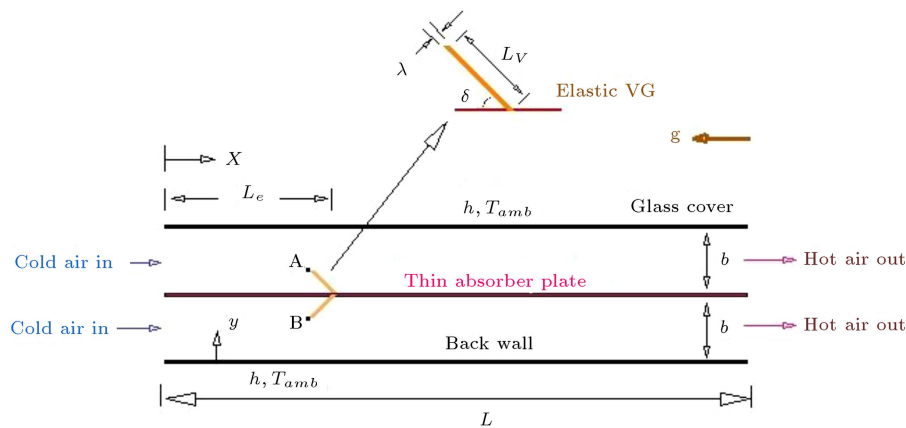


**Figure 1.** Geometry of air heater ( $b = 4$  cm,  $L = 100$  cm); points A and B are on the tips of VGs.

### 3.1. Governing differential equation

In the numerical simulation, the following flow equations were simultaneously solved in their RANS forms including the continuity, momentum, and energy with the Boussinesq approximation coupled with the governing equations of the motion of EVG according to the FSI.

$$\frac{D\rho}{Dt} + \rho \nabla \cdot V = 0, \tag{1}$$

$$\begin{aligned} \frac{D}{Dt}(\rho V) = -\nabla p + \nabla \cdot [(\mu + \mu_t)(\nabla V + \nabla V^T)] \\ + (\rho - \rho_0)g - \nabla \cdot \left(\frac{2}{3}\mu \nabla \cdot V\right) + F_{ext, VG}, \end{aligned} \tag{2}$$

$$\frac{D(\rho c_p T)}{Dt} = \nabla \cdot \left[ (k_{th} + \frac{c_p \mu_t}{Pr_t}) \nabla T \right], \tag{3}$$

$$\frac{D(\rho k)}{Dt} = \nabla \cdot \left[ \left( \mu + \frac{\mu_t}{\sigma_k} \right) \nabla k \right] + P_k + P_b - \rho \varepsilon + S_k, \tag{4}$$

$$\begin{aligned} \frac{D(\rho \varepsilon)}{Dt} = \nabla \cdot \left[ \left( \mu + \frac{\mu_t}{\sigma_\varepsilon} \right) \nabla \varepsilon \right] + C_1 \frac{\varepsilon}{k} (P_k + C_3 P_b) \\ - C_2 \rho \frac{\varepsilon^2}{k} + S_\varepsilon, \end{aligned} \tag{5}$$

where  $\mu_t = C_\mu \frac{\rho k^2}{\varepsilon}$  is the turbulent viscosity,  $C_1$ ,  $C_2$ , and  $C_3$  are the constants, and  $P_k$  and  $P_b$  denote the productions of turbulence and buoyancy, respectively. In addition,  $F_{ext, VG}$  is the external force produced by the FSI [24,25]. The  $k - \varepsilon$  method was used for turbulence modeling. More details are given in Tables 2 and 3. The FSI formulation for  $F_{ext, VG}$  computation is provided by the COMSOL Multi-physics Inc. [25] based on the relations given in [26].

### 3.2. Boundary condition

Both initial and boundary conditions are required in the numerical solution of the governing differential equations in unsteady conditions. For the present simulated problem, these conditions are summarized below:

- At the initial time, the air is at ambient temperature under a stagnant condition;
- At both inlet and outlet of the heater duct, the air flow is at zero-gauge pressure;

**Table 3.** Minimum values of residuals.

Mass	Momentum	Energy
$5 \times 10^{-5}$	$10^{-4}$	$5 \times 10^{-4}$

- According to the no-slip condition, zero velocity is considered at the gas-solid interfaces;
- The working gas temperature at the outlet section is updated by the energy balance criterion, while zero axial gradients are used for all other dependent variables;
- Constant heat flux of  $640 \text{ W/m}^2$  is imposed on the absorber, while the convection boundary condition with  $h = 5 \text{ W/m}^2\text{K}$  and  $T_{amb} = 293 \text{ K}$  is applied to the boundary walls (Figure 1).

### 4. Mesh

In order to mesh the computational domain, the unstructured triangular grid shown in Figure 2 was

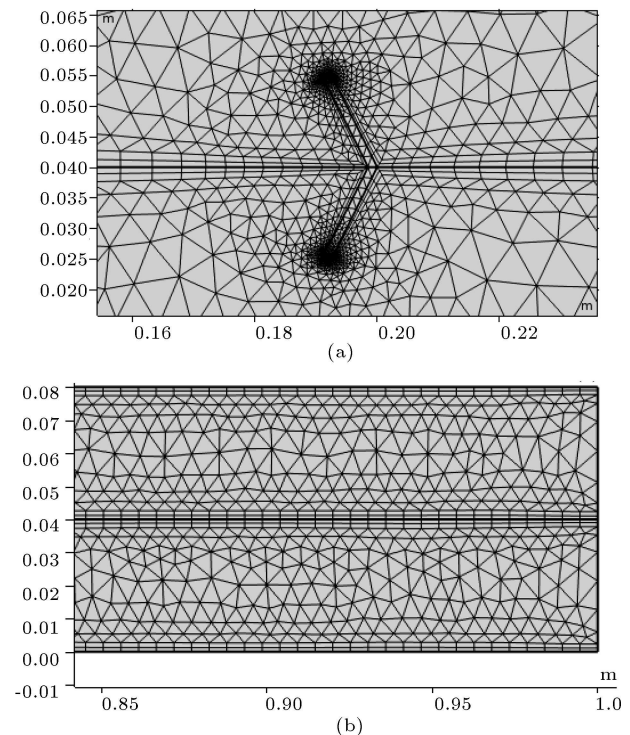


**Figure 2.** Discretized computational domains: (a) Zoomed discretized domain near the VG and (b) refined mesh near the wall.

**Table 2.** Methodology in simulation.

Regime of flow	Turbulence modeling	Algorithm	Ra	Re
Turbulent	Standard $k - \varepsilon$	SIMPLE	$10^{11} - 10^{12}$	3000-4000
$C_1$	$C_2$	$C_3$	$\sigma_\varepsilon$	$\sigma_k$
1.44	1.92	0.09	1.3	1.0

**Table 4.** Mesh dependency check.

No. of elements	8900		12400		16700		19900	
	Value	Change	Value	Change	Value	Change	Value	Change
<b>Flow rate (m<sup>2</sup>/s)</b>	0.0270	–	0.0319	18%	0.0330	3%	0.0332	0.6%

used due to the existence of VG in SAH. According to the mesh independency test, the grid size with 16700 elements and average element quality of 0.93 constituted an optimum grid. In the grid-dependent study, the values of natural airflow rates of different mesh sizes were calculated, results of which are given in Table 4. According to this table, using a mesh better than the optimum one did not have any considerable variation in the computed air flow rate. Consequently, the discretized domain with 16700 elements was used in all subsequent calculations.

## 5. Validation

To validate the present simulation, the numerical finding was compared with the experimental data given in [27]. A vertical duct with free convection airflow was simulated for this purpose. It is rectangular in shape with the height and width of 8 m and 0.5 m, respectively. The temperature of the heated wall was 423 K, and the other side of the wall was kept in an adiabatic condition. The ambient temperature was 20°C and the free convective flow was turbulent given that  $Ra = 5 \times 10^{12}$ . Figure 3 shows the temperature and velocity distributions along the  $x$ -direction at  $y = 7.8$  m and makes a comparison between these findings and the experimental results. This figure confirms good consistency between the computed velocity and temperature fields and the experimental data.

In the second test case, a forced convection airflow in a duct with two heated walls was simulated in the presence of a flapping VG. This FSI problem was studied before by Li et al. [14] based on a theoretical method. The variations in the average Nusselt numbers along the bottom wall at different Reynolds numbers and moduli of elasticity are given in Figure 4. The computed Nusselt number was defined based on the average heat transfer coefficient and duct hydraulic diameter.

As observed in this figure, there is good agreement between the results of the present FEM simulation and those obtained by Li et al. [14]. The VG elasticity varies from the infinite value corresponding to the rigid body to 0.4 MPa known as high-elastic material. Given that the value of VG elasticity has a considerable effect on the flow field, very good agreement in a wide elasticity range points to the reliability of all involved numerical procedures.

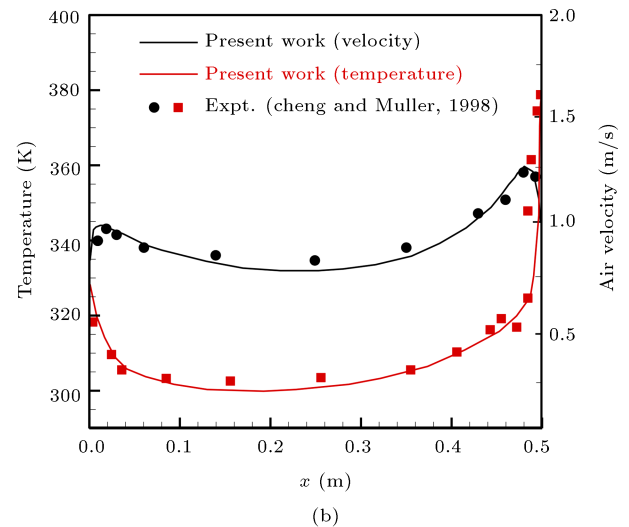
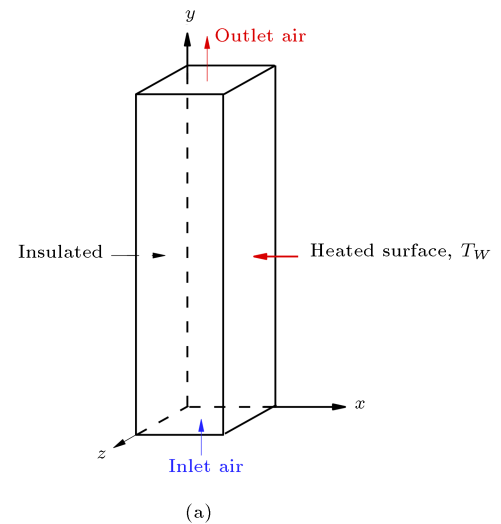


**Figure 3.** (a) Geometry of the studied chimney in [27]. (b) Velocity and temperature distributions at  $y = 7.8$  m.

## 6. Results

This section presents the numerical results of the present simulations of the transient turbulent natural convection in a planar SAH. First, the trends of the residuals of the governing equations that are usually used as the convergence criteria are depicted in Figure 5. As observed, the numerical error of all governing equations falls below  $10^{-4}$ , thus ensuring the good convergence of the governing equations. In addition, the airflow rate and outlet temperature of three SAH

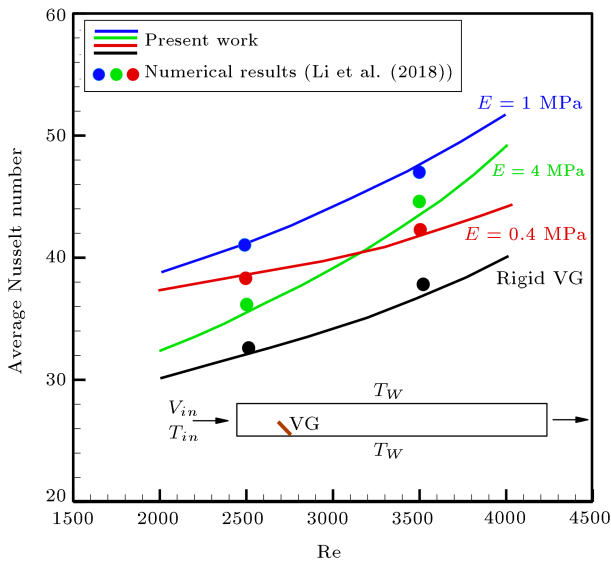


**Figure 4.** Average value of Nu along the lower wall for different values of Re and moduli of elasticity [14].

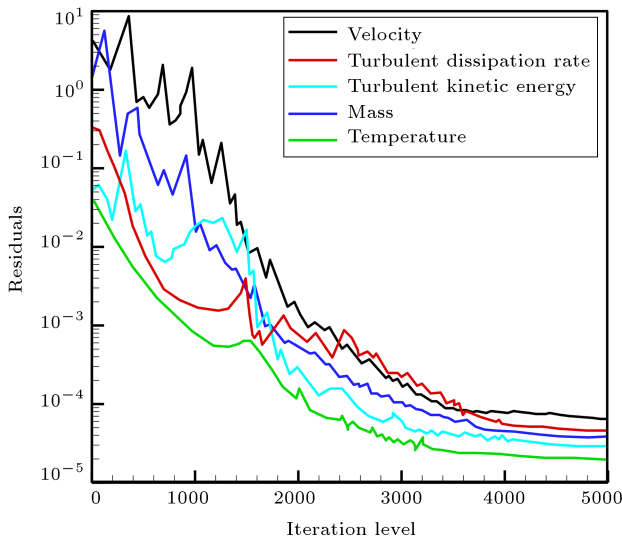


**Figure 5.** Variation in the residual of equations vs. iteration.

configurations: (a) SAH + EVG, (b) SAH + RVG, and (c) CSAH are given.

**6.1. SAH with EVG**

Figure 6 shows the contours of air velocity magnitude at different times. Obviously, as the absorber receives the solar heat flux, its temperature rises, thus making the adjacent quiescent air warm. Once the air warms up, its density decreases and the buoyant body force pushes it towards the outlet. In the lower part of the SAH, however, the embedded EVG does not allow air to pass and blocks its way until its momentum becomes strong enough to turn over the inclined EVG. The airflow passes over the EVG for the first time at  $t = 1.5$  s. Half a second later, the first vortices

behind the EVGs are formed at  $t = 2.0$  s as the airflow is reattached to the heated absorber wall. As a result of the EVG vibration, a new dynamic of the wavy flow field is formed right after the EVG through both passages along the SAH. The generated flow vortices and airflow in the wavy form are known to be responsible for mixing the process and heat transfer augmentation, and the repeated hydraulic behavior observed at  $t = 9$  s as well as Figures 6 and 7 is called Periodic Steady State (PSS).

A closer look at the flow field, particularly in periodic steady states, e.g., the time after 7 s is indicative of the outstanding functionality of the EVG. As observed, the flow field before the EVG is distinguished from the flow field after the EVG. Not only is the parallel laminated flow turned into a wavy flow fluid containing moving vortices, but also the nearly uniform velocity is turned into a non-uniform profile with a core of high-magnitude velocity. After the EVG, it is this high-velocity airflow that bounces up and down on the absorber that causes heat transfer enhancement. In fact, the EVG leads to a higher Reynolds number locally, which has a better thermal effect in the case of wavy uniform flow.

The functionality of the EVG in generating the vortices is not clear in Figure 6. In this regard, Figure 7 is presented to clarify this functionality that illustrates the streamlines of the flow field together with the contour of velocity magnitude in a zoomed area of one pass. The flow behavior was captured at a time step of  $\Delta t = 0.5$  s. The new fluid dynamics induced by the embedded EVG was found with moving vortices marching toward the outlet section.

Figure 8 displays the contour of temperature along the SAH whose periodic pattern is clearly illustrated at  $t = 10.0$  s. The maximum temperature was observed at the attached point of the EVG and heated wall as well as the area inside the recirculated zones downstream of VGs. Figure 8 clarifies the mixing effect of EVG which leads to breaking the thermal boundary layer and enhancing the convection heat transfer. The non-uniform velocity profile of the wavy flow field causes more penetration of the heat from the absorber across the channel while dissipating and fading gradually. Flow impingement onto the absorber plate in the temperature contour can be detected where the high-temperature boundary layer becomes thinner.

The pressure contour at a PSS time of  $t = 10.0$  s is drawn in Figure 9 where the maximum variation of pressure is only 0.6 Pa (from  $-0.55$  to  $0.05$ ) which is a negligible value. Moreover, due to the low-speed attached wake downstream of the VG, air pressure drops even below the outlet pressure. This negative pressure is also responsible for the formation of recirculation zone behind the EVG.

Figure 10 presents the quantitative estimation of

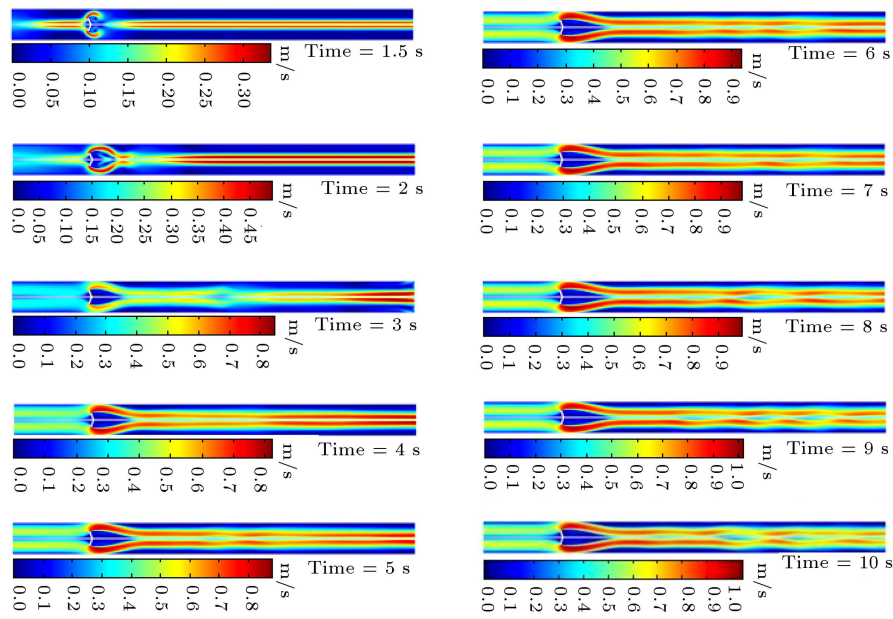


Figure 6. The contours of air velocity magnitude from the initial time up to PSS.

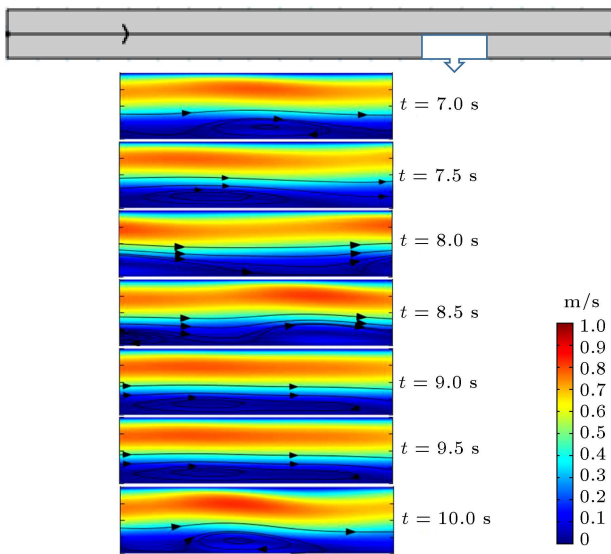


Figure 7. Demonstration of moving vortex by streamlines in a zoomed area captured at different times.

the buoyant body force which has the main role in generating free convection flow.

As observed, the buoyant force was initiated right adjacent to the heated absorber wall. It evolves gradually whose maximum value reaches  $2 \text{ N/m}^3$  close to and behind the EVG while its minimum value, i.e., zero  $\text{N/m}^3$ , occurs far from the heated wall and near the transparent wall in contact with the ambient free convection. Corresponding to the amount of deflection along the EVG, stress is created within this element. Von Mises stress is a well-known stress parameter that is usually used to predict whether or not the material will be either obtained or fractured under a

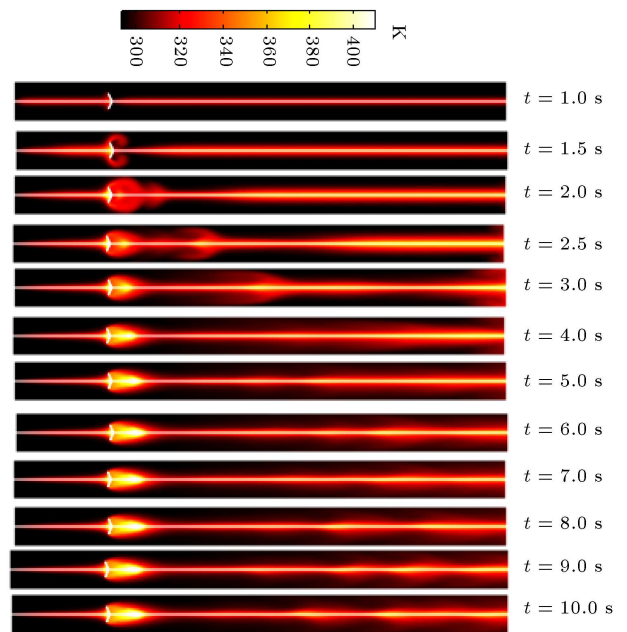


Figure 8. Evolution of temperature contour at different times for the DP-SAH with EVG up to PSS.

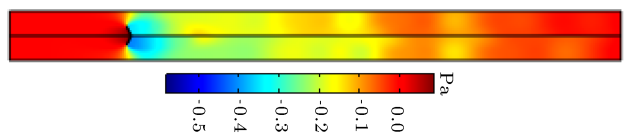


Figure 9. Air pressure at  $t = 10 \text{ s}$  for the SAH with EVG.

specific load. Figure 11 shows the von Mises stress contour inside the EVG at PSS. From the structural mechanics point of view, the EVG can be considered an elastic cantilever beam where the impact of the

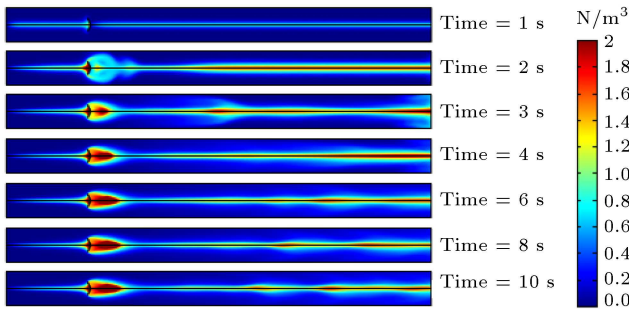


Figure 10. The body force contour at different times.

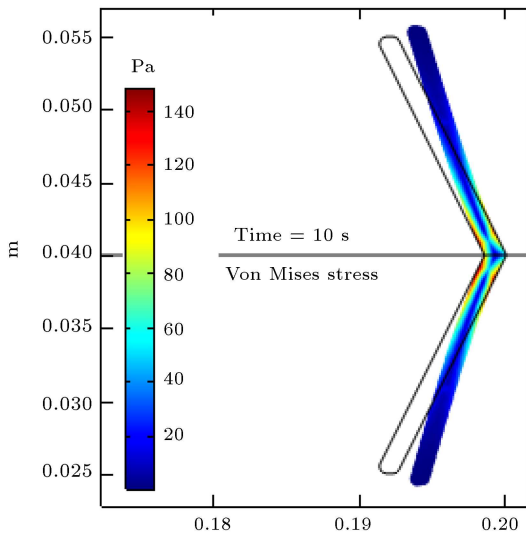


Figure 11. The von Mises stress contour within the EVG.

airflow momentum on the EVG would appear as a bending moment. This moment causes both shear and normal stresses such that their combination based on the maximum distortion criterion for ductile material is formulated for the analysis of plastic deformation. As observed, the maximum von Mises stress of 140 Pa occurs close to the attached point of EVG to the absorber wall on the outer surface of EVG, the further point to the neutral axis. This maximum value of von Mises stress corresponds to 2.6 mm displacement of the EVG tip.

**6.2. Comparison of different configurations**

For a more detailed evaluation of the effect of vortex generation on the SAH performance, extensive comparisons were made for the generated flow rate, outlet bulk temperature, and absorber wall temperature. From now on, the SAH without VG is referred to as Clear SAH (CSAH). Figure 12 shows the time history of the airflow rate in the outlet section for three different configurations: (a) SAH+EVG, (b) SAH+RVG, and (c) CSAH. According to this figure, the buoyant force drives the stagnant air into motion such that the distribution of air flowrate with time follows almost the same trend for all configurations. The PSS average

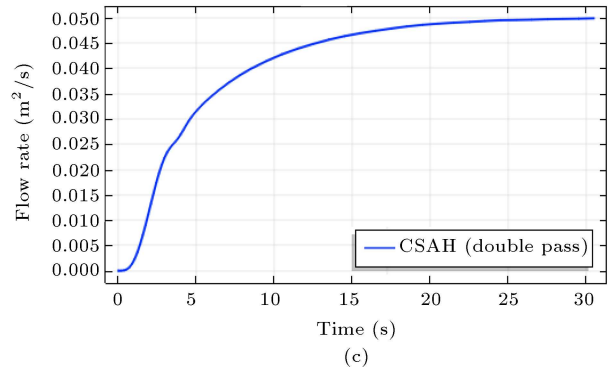
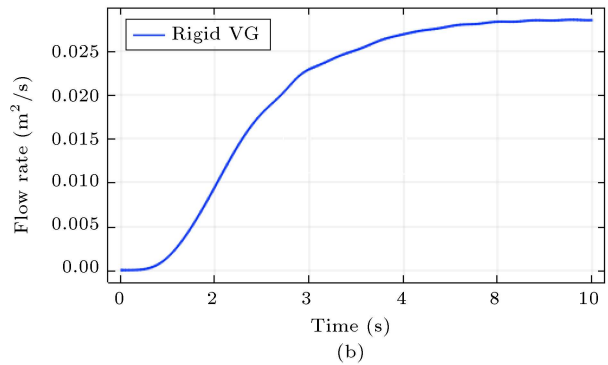
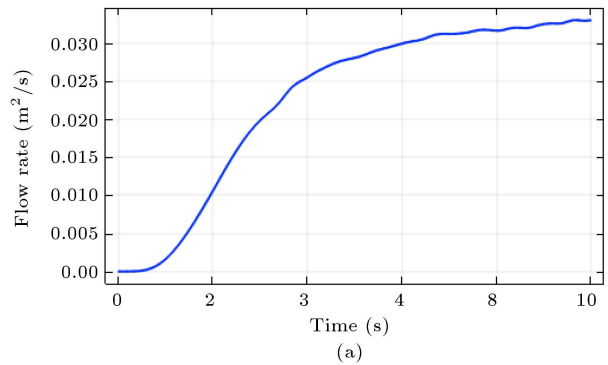


Figure 12. Variations in the airflow rates over time for different configurations: (a) SAH + EVG, (b) SAH + RVG, and (c) CSAH.

value of the flowrate for three configurations is given in Table 5. Of note, configurations (c) and (b) have the highest and lowest flow rates among all other configurations, respectively. The CSAH configuration has no obstacle in front of airflow and consequently, it has maximum flowrate. Figure 12 and Table 5 together show that the effect of RVG blockage is greater than that of EVG.

Application of RVG instead of its elastic counterpart will decrease the flow rate by 15.6% implying that RVG has 15.6% greater blockage effect due to the lack of flexibility against the initiative airflow than its elastic version, thus reducing the acceleration of the flow toward its steady-state value. From the beginning of the numerical experiment for all configurations, the

**Table 5.** The averaged values of airflow rate for three configurations in PSS condition.

Configurations	(a) SAH+EVG	(b) SAH+RVG	(c) CSAH
PSS value of flow rate (m <sup>2</sup> /s)	0.033	0.028	0.050
Percentage of reduction with respect to (c)	-33.6%	-44%	-
Percentage of enhancement with respect to (a)	-	-15.6 %	50.6 %

**Table 6.** The PSS averaged value of OBT for three configurations.

	Configurations		
	(a) SAH+EVG	(b) SAH+RVG	(c) CSAH
PSS averaged value of OBT (°C)	40	40	33
$\Delta\bar{T} = \bar{T}_{out} - T_{in}$ (°C)	20	20	13
$\Delta\bar{T}$ enhancement with respect to (c) (%)	53.8%	53.8%	-
Maximum recorded OBT (°C)	59	57	57

flow rate is zero until approximately  $t = 0.6$  s that takes working gas to warm up and makes the body force strong enough to initiate the flow rate.

The following illustration on Outlet Bulk Temperature (OBT), depicted in Figure 13, reveals the physics behind heat transfer enhancement in the complicated phenomenon of vortex generation in transient turbulent natural convection. Figures 10 and 11 should be interpreted together since their physics is strongly interlaced. At the starting time, the incoming solar heat flux is absorbed by the absorber wall that causes a high temperature difference between the absorber and air layers. The body force due to this effect drives the neighboring bulk of fluid faster. An increase in velocity then causes a decrease in the temperature of absorber. Therefore, the air outlet temperature must have a maximum value that takes place close to the starting time between  $t = 2$  s and  $t = 4$  s. The maximum recorded OBT is attributed to the SAH with EVG. Moreover, in clean SAH, temperature fluctuation disappears since there is no reason to disturb the airflow. Those configurations equipped with VG show fluctuation over time. However, SAH with EVG shows more fluctuations due to its flexibility and winglet elasticity with respect to the RVG.

Followed by this maximum value and as a result of the EVG oscillation, the OBT experiences fluctuating behavior until reaching PSS, where the OBT asymptotically approaches its final value at which a repetitive trend can be observed in the outlet section. Tables 5 and 6 were taken into consideration at the same time to make an overall conclusion; that is, in the case of SAH of PDP type, the RVG, in comparison with its competitor, the EVG, has the same thermal performance, but exhibits 15.6% less hydraulic efficiency. In order to compare the performances of SAHs with different configurations, the outlet bulk temperature difference is defined as  $\Delta\bar{T} = \bar{T}_{out} - T_{in}$  where  $\bar{T}_{out}$  is the time-averaged value of the outlet temperature

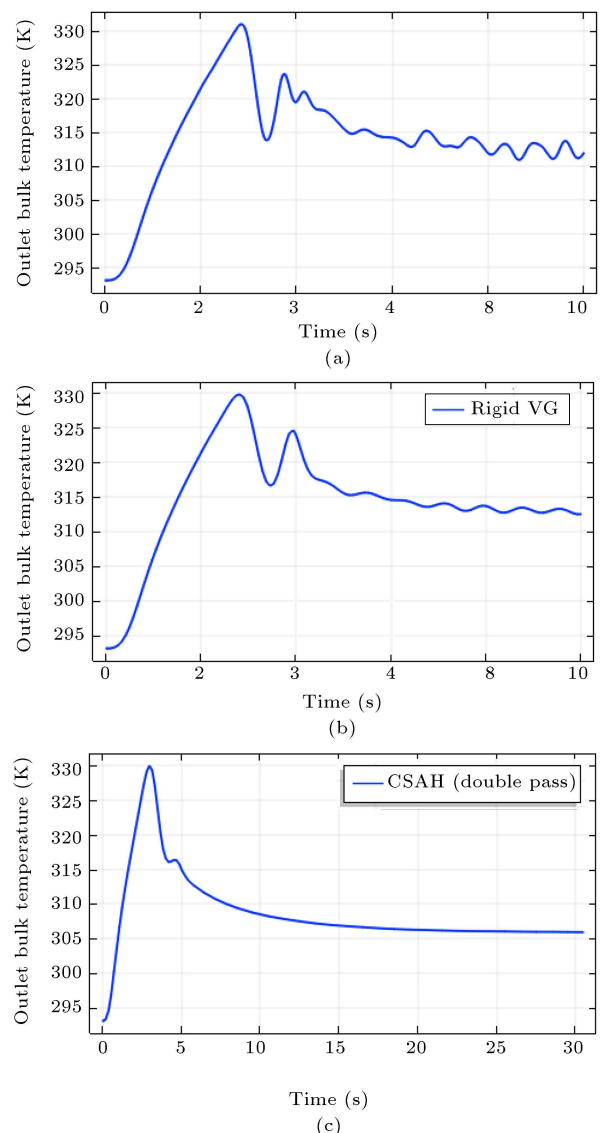


**Figure 13.** Variations in the OBT over time for different configurations: (a) SAH + EVG, (b) SAH + RVG, and (c) CSAH.

in the PSS condition. Upon computing the value of the temperature difference of the outlet bulk for a conventional clear SAH and comparing it with its corresponding value for SAH with VG, we found that the proposed configuration exhibited a 53.8% increase in the outlet temperature [from 13 to 20°C] while reducing the rate of airflow by 33.6% [from 0.033 to 0.050 m<sup>2</sup>/s].

Another way to point out the heat transfer enhancement, especially where there is constant heat flux, is to determine the heated-wall temperature. Better heat transfer leads to lower wall temperature, hence a better evaluation of the proposed methodology. Figure 14 shows the absorber wall temperature at different times,  $t = 1, 3, 5,$  and  $10$  s, for different

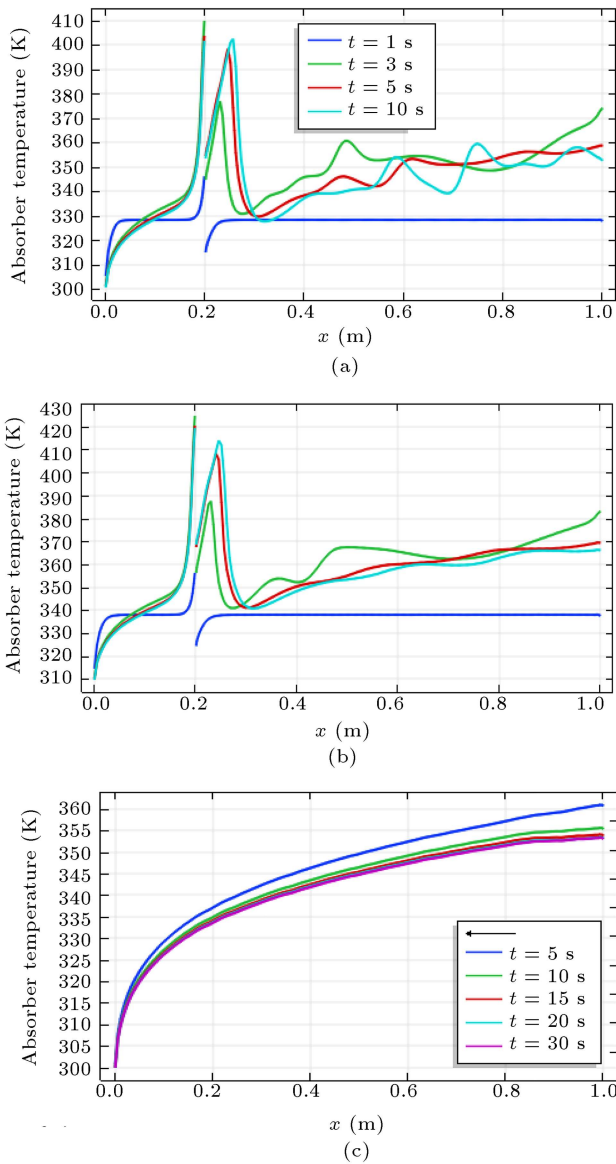


**Figure 14.** Variations in the absorber wall temperatures at different times and different configurations: (a) SAH+EVG, (b) SAH+RVG, and (c) CSAH.

configurations of (a)-(c), respectively. Except for case (c) where SAH has no VG, the other two cases follow almost the same trend. In case (c), the flow field is planar and the streamlines are almost parallel and consequently, heat transfer is approximately pure conduction whose direction is perpendicular to the flow direction. In addition, the thermal boundary layer grows along the wall and becomes thicker, and air temperature along and adjacent to the wall becomes hotter, indicating that heat transfer is decreasing along the absorber wall. Consequently, a monotonic increase in the temperature along the wall can be expected. In SAH with EVG/RVG, the temperature of the wall considerably increases locally due to the stagnation point where air is trapped in an acute angled corner, while after the EVG/RVG, it exhibits an oscillating behavior until the outlet section.

The above-mentioned claim on the fluctuating flow field can be evaluated by the displacement variation at the tip of EVG, i.e., Points A and B, as depicted in Figure 15. Among these three configurations mentioned earlier, SAH+RVG and CSAH have no displacement mainly because in the former, the VG is considered rigid, and the latter has no VG. This is the main reason why just the first configuration is discussed here. Earlier, the EVG is almost without considerable movement while the initial airflow adjacent to the hot surface is already begun. In this stage, the fluid momentum is not strong enough to bend EVG and pass it over. Upon increasing the buoyant body force resulting from more temperature difference between the working gas and absorber, the convective flow would turn around the EVG and pass it over. At this moment, the fluid momentum bends the tip of the EVG up to 0.6 mm at  $t = 2.0$  s. After this peak, the innate elasticity of the EVG is forced to turn the deformed shape back while the momentum of air flow resists it. Moreover, at the interval of  $t = 4$  to  $9$  s, the displacements of EVG in two parallel passes deviate a little and do not match exactly. This small deviation makes the flow fields in two passes non-

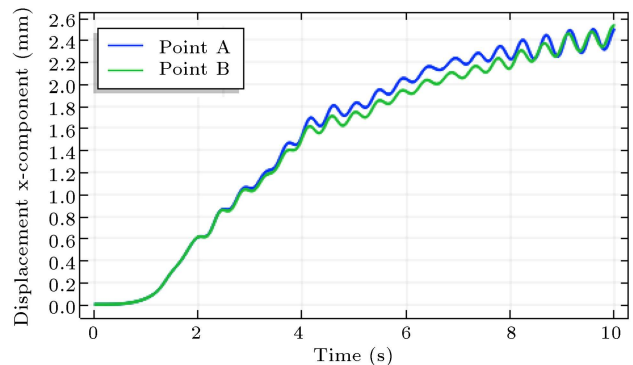


**Figure 15.** Variations in the x-component of the displacements of VGs at their tips.

symmetrical. However, after  $t=9$  s, their vibrations overlapped perfectly. The EVG actions and airflow reactions lead to transient vibrations of EVG and wavy dynamic of airflow through the passes.

## 7. Conclusion

This study aimed to enhancing the thermal performance of a parallel double-pass Solar Air Heater (SAH) by embedding elastic winglets as the vortex generators inside the heater chimney attached to the absorber surface on both passages. In the novel design of SAH, the passive method induced new active dynamics into the flow field. In addition, this study presented an extensive thermo-hydrodynamic analysis of turbulent free convection coupled with Fluid Solid Interaction (FSI). Comparisons between the reported experimental and theoretical data and the present numerical findings showed very good consistency. The set of numerical experiments of the current study revealed a considerable increase in the thermal efficiency of the proposed novel SAH with two Elastic Vortex Generators (EVGs), given that it offered a higher outlet temperature with respect to the conventional clean SAH. The rigid VG, in comparison with its competitor, the EVG, had the same outlet temperature, yet its hydraulic efficiency was 15.6% less than that of its competitor. The outlet bulk temperature difference was defined as  $\Delta\bar{T} = \bar{T}_{out} - T_{in}$ , and its value was compared with that of a conventional clear SAH. As a result, embedding EVG inside SAH caused 53.8% improvement in the air temperature increase [from 13°C to 20°C] through the SAH while reducing 33.6% in air flow rate [from 0.033 m<sup>2</sup>/s to 0.050 m<sup>2</sup>/s].

## Nomenclature

$b$	Air layer thickness (m)
$c_p$	Specific heat capacity (kJ/kg K)
$g$	Acceleration of gravity (m.s <sup>-2</sup> )
$h$	Coefficient of convection (W/m <sup>2</sup> K)
$k_{th}$	Conductivity (Wm <sup>-1</sup> K <sup>-1</sup> )
$L$	Length (m)
$n$	Normal direction
$\dot{m}$	Mass flow rate (kg/s)
$Pr$	Prandtl number (-)
$q$	Heat flux (W/m <sup>2</sup> )
$Ra$	Rayleigh number (-)
$Re$	Reynolds number (-)
$t$	Time (s)
$T$	Temperature (K)
$V$	Flow velocity (m/s)

$P$	Pressure (Pa)
$(x, y)$	Coordinate system (m)
$\alpha$	Thermal diffusivity (m <sup>2</sup> /s)
$\delta$	Attacked angle
$\varepsilon$	Turbulent dissipation
$\kappa$	Turbulence kinetic energy (m <sup>2</sup> /s <sup>2</sup> )
$\mu$	Viscosity (Pa.s)
$\rho$	Air density (kg/m <sup>3</sup> )

## Abbreviation

SAH	Solar Air Heater
SHF	Solar Heat Flux
PDP	Parallel Double Pass
PSS	Periodic Steady State
OBT	Outlet Bulk Temperature
EVG	Elastic Vortex Generator
RVG	Rigid Vortex Generator
CSAH	Clean SAH (SAH without any kind of VG)

## References

1. BP group, BP Energy Outlook 2030 (2013).
2. Gill, R.S., Singh, S., and Singh, P.P. "Low cost solar air heater", *Energy Convers. Manag.*, **57**, pp. 131–142 (2012).
3. Tuncer, A.D., Khanlari, A., Sözen, A., et al. "Energy-exergy and enviro-economic survey of solar air heaters with various air channel modifications", *Renew. Energy*, **160**, pp. 67–85 (2020).
4. Singh, A.P. and Singh, O.P. "Thermo-hydraulic performance enhancement of convex-concave natural convection solar air heaters", *Sol. Energy*, **183**, pp. 146–161 (2019).
5. Rayeni, A.D. and Gandjalikhan Nassab, S.A. "Effects of gas radiation on thermal performances of single and double flow plane solar heaters", *Int. J. Eng.*, **33**, pp. 1156–1166 (2020).
6. Foruzan Nia, M., Gandjalikhan Nassab, S.A., and Ansari, A.B. "Numerical simulation of flow and thermal behavior of radiating gas flow in plane solar heaters", *J. Therm. Sci. Eng. Appl.*, **12**, pp. 031008–1 (2020).
7. Vijayan, S., Arjunan, T.V., Kumar, A., et al. "Experimental and thermal performance investigations on sensible storage based solar air heater", *J. Energy Storage*, **31**, p. 101620 (2020).
8. Ghritlahre, H.K. and Verma, M. "Accurate prediction of exergetic efficiency of solar air heaters using various predicting methods", *J. Clean. Prod.*, **288**, p. 125115 (2020).

9. Yadav, S. and Saini, R.P. “Numerical investigation on the performance of a solar air heater using jet impingement with absorber plate”, *Sol. Energy*, **208**, pp. 236–248 (2020).
10. Korpale, V.S., Deshmukh, S.P., Mathpati, C.S., et al. “Numerical simulations and optimization of solar air heaters”, *Appl. Therm. Eng.*, **180**, p. 115744 (2020).
11. Sheikhnejad, Y. and Gandjalikhan Nassab, S.A. “Enhancement of solar chimney performance by passive vortex generator”, *Renew. Energy*, **169**, pp. 437–450 (2021).
12. Shi, J., Hu, J., Schafer, S.R., et al. “Numerical study of heat transfer enhancement of channel via vortex-induced vibration”, *Appl. Therm. Eng.*, **70**, pp. 838–845 (2014).
13. Fiebig, M. “Vortices, generators and heat transfer”, *Chem. Eng. Res. Des.*, **76**, pp. 108–123 (1998).
14. Li, Z., Xu, X., Li, K., et al. “A flapping vortex generator for heat transfer enhancement in a rectangular airside fin”, *Int. J. Heat Mass Transf.*, **118**, pp. 1340–1356 (2018).
15. Ali, S., Menanteau, S., Habchi, C., et al. “Heat transfer and mixing enhancement by using multiple freely oscillating flexible vortex generators”, *Appl. Therm. Eng.*, **105**, pp. 276–289 (2016).
16. Soti, A.K., Bhardwaj, R., and Sheridan, J. “Flow-induced deformation of a flexible thin structure as manifestation of heat transfer enhancement”, *Int. J. Heat Mass Transf.*, **84**, pp. 1070–1081 (2015).
17. Park, S.G., Kim, B., Chang, C.B., et al. “Enhancement of heat transfer by a self-oscillating inverted flag in a Poiseuille channel flow”, *Int. J. Heat Mass Transf.*, **96**, pp. 362–370 (2016).
18. Favier, J., Revell, A., and Pinelli, A. “Numerical study of flapping filaments in a uniform fluid flow”, *J. Fluids Struct.*, **53**, pp. 26–35 (2015).
19. Varol, Y. and Oztop, H.F. “A comparative numerical study on natural convection in inclined wavy and flat-plate solar collectors”, *Build. Environ.*, **43**, pp. 1535–1544 (2008).
20. Varol, Y., Koca, A., Oztop, H.F., et al. “Forecasting of thermal energy storage performance of phase change material in a solar collector using soft computing techniques”, *Expert Syst. Appl.*, **37**, pp. 2724–2732 (2010).
21. Bayrak, F., Oztop, H.F., and Hepbasli, A. “Energy and exergy analyses of porous baffles inserted solar air heaters for building applications”, *Energy Build.*, **57**, pp. 338–345 (2013).
22. Oztop, H.F., Bayrak, F., and Hepbasli, A. “Energetic and exergetic aspects of solar air heating (solar collector) systems”, *Renew. Sustain. Energy Rev.*, **21**, pp. 59–83 (2013).
23. Singh, A.P., Kumar, A.A., and Singh, O.P. “Designs for high flow natural convection solar air heaters”, *Sol. Energy*, **193**, pp. 724–737 (2019).
24. Tallec, P.L. and Mouro, J. “Fluid structure interaction with large structural displacements”, *Comput. Methods Appl. Mech. Eng.*, **190**, pp. 3039–3067 (2001).
25. *Comsol Multiphysics, ALE Fluid-Structure Interaction*, pp. 1–16 (2011).
26. Zienkiewicz, O.C., Taylor, R., and Nithiarasu, P., *The Finite Element for Fluid Dynamic*, 7th edition, pp. 50–88, Butterworth-Heinemann Press, Oxford, Uk (2006).
27. Cheng, X. and Müller, U. “Turbulent natural convection coupled with thermal radiation in large vertical channels with asymmetric heating”, *Int. J. Heat Mass Transf.*, **41**, pp. 1681–1692 (1998).

## Biographies

**Seyyed Abdolreza Gandjalikhan Nassab** is a Professor at the Mechanical Engineering Department at Shahid Bahonar University of Kerman, Iran. He obtained his PhD from Shiraz University in 1999. He has several published papers on radiation and convection heat transfer. Currently, he is working on many more papers. His other areas of specialization include tribology and CFD.

**Yahya Sheikhnejad** is a Postdoc researcher fellow at the Department of Mechanical Engineering at University of Aveiro, Portugal. He obtained his PhD from Amirkabir University of Technology in 2016. He has some papers on fluid mechanics and heat transfer and participated in several high-profile conferences.